PAR-4 and anillin regulate myosin to coordinate spindle and furrow position during asymmetric division

Anne Pacquelet,[1,2] Perrine Uhart,[1,2] Jean-Pierre Tassan,[1,2] and Grégoire Michaux[1,2]

[1]Centre National de la Recherche Scientifique, UMR6290, Rennes, France
[2]Université de Rennes 1, Institut de Génétique et Développement de Rennes, 35043 Rennes, France

During asymmetric cell division, the mitotic spindle and polarized myosin can both determine the position of the cytokinetic furrow. However, how cells coordinate signals from the spindle and myosin to ensure that cleavage occurs through the spindle midzone is unknown. Here, we identify a novel pathway that is essential to inhibit myosin and coordinate furrow and spindle positions during asymmetric division. In *Caenorhabditis elegans* one-cell embryos, myosin localizes at the anterior cortex whereas the mitotic spindle localizes toward the posterior. We find that PAR-4/LKB1 impinges on myosin via two pathways, an anillin-dependent pathway that also responds to the cullin CUL-5 and an anillin-independent pathway involving the kinase PIG-1/MELK. In the absence of both PIG-1/MELK and the anillin ANI-1, myosin accumulates at the anterior cortex and induces a strong displacement of the furrow toward the anterior, which can lead to DNA segregation defects. Regulation of asymmetrically localized myosin is thus critical to ensure that furrow and spindle midzone positions coincide throughout cytokinesis.

Introduction

During asymmetric cell division, establishment of a polarity axis and proper orientation of the mitotic spindle before mother cell division are key steps to allow the unequal inheritance of cell fate determinants between the two daughter cells (Knoblich, 2010). Asymmetric cell division often leads to size asymmetry of the daughter cells, implying that the spindle midzone is not symmetrically positioned within the mother cell. In some instances, such as in the one-cell *Caenorhabditis elegans* embryo, the spindle is built in a symmetric manner and pulled toward one side of the mother cell (Knoblich, 2010). Other asymmetrically dividing cells, such as *Drosophila melanogaster* neuroblasts, have a spindle that elongates asymmetrically (Knoblich, 2010). In both cases, it is critical that the cytokinetic furrow aligns with the spindle midzone to ensure both asymmetric cell division and proper DNA segregation. Two pathways have been shown to coordinate spindle and furrow positions by inducing cytokinesis furrow formation in the vicinity of the spindle midzone: the centralspindlin and the astral microtubule pathway (Dechant and Glotzer, 2003). The centralspindlin complex, formed by the kinesin MKLP-1/ZEN-4 and MgcRacGAP/CYK-4, is localized at both the spindle midzone and the equatorial cortex where it triggers the accumulation of active RhoA and contractile ring components (Yüce et al., 2005; Nishimura and Yonemura, 2006; Basant et al., 2015). Astral microtubules have been proposed to inhibit the accumulation of contractile ring proteins at the poles of the dividing cell (Werner et al., 2007; Lewellyn et al., 2010).

A spindle-independent furrowing mechanism has also been described in *Drosophila* and *C. elegans* neuroblasts (Cabernard et al., 2010; Ou et al., 2010). In these cells, myosin accumulates asymmetrically at the cell cortex during early anaphase. It then drives furrow contraction and asymmetric elongation of the spindle. As a consequence, neuroblasts divide asymmetrically, giving rise to a smaller daughter cell on the side on which myosin has accumulated. The ability of myosin to induce cytokinesis suggests the existence of regulatory mechanisms to prevent it from inducing cytokinesis in an inappropriate manner. Such regulation may be particularly critical in cells in which myosin localization does not correlate with spindle position and where furrow localization may thus result from a tug-of-war between the signals emanating from myosin and the spindle.

The one-cell *C. elegans* embryo is a well-established model to study the different aspects of asymmetric cell division. After fertilization, myosin II (NMY-2) flows toward the anterior pole of the embryo and leads to the asymmetric distribution of polarity proteins: PAR-3, PAR-6, and PKC-3 accumulate at the anterior cortex, whereas PAR-2 and PAR-1 localize at the posterior cortex (Kemphues, 2000; Munro et al., 2004). Independently of myosin, posterior microtubules also contribute to the posterior accumulation of PAR-2 (Motegi et al., 2011). In turn, polarity proteins control the forces that are exerted on the mitotic spindle to pull it toward the posterior pole of the embryo

Correspondence to Anne Pacquelet: anne.pacquelet@univ-rennes1.fr

Abbreviations used in this paper: DIC, differential interference contrast; P-MLC, phosphorylated myosin light chain.

The Rockefeller University Press $30.00
J. Cell Biol. Vol. 210 No. 7 1085–1099
www.jcb.org/cgi/doi/10.1083/jcb.201503006

(Grill et al., 2001). The centralspindlin and astral microtubule pathways then induce cytokinesis (Dechant and Glotzer, 2003), and the furrow ingresses through the spindle midzone and gives rise to a large anterior cell (AB) and a small posterior cell (P1). In contrast to what happens in neuroblasts, furrow ingression occurs in the posterior half of the embryo, despite myosin being present at the anterior cortex.

Another essential PAR protein, the kinase PAR-4/LKB1, uniformly localizes at the one-cell embryo cortex and mildly modulates the establishment of polarity through the regulation of actomyosin contractions and anillins (Morton et al., 1992; Watts et al., 2000; Chartier et al., 2011). *Drosophila* and mammalian anillin interact with nonmuscle myosin and several essential players of cytokinesis, including septins, the centralspindlin subunit MgcRacGAP/CYK-4, and RhoA (Piekny and Maddox, 2010). In *C. elegans,* the anillin ANI-1 carries all the characteristic binding domains of anillin and is required for cortical actomyosin contractility during polarity establishment; it is also present at the cytokinesis furrow (Maddox et al., 2005). ANI-2 is a shorter form of anillin that lacks the N-terminal actin and myosin binding domains. During polarity establishment, PAR-4 positively regulates actomyosin contractions by inhibiting ANI-2, which in turn has been proposed to inhibit ANI-1, possibly by acting as a competitor (Chartier et al., 2011; Amini et al., 2014).

Here we identify a novel regulatory pathway that is essential to maintain a low level of myosin at the anterior cortex during cytokinesis and we find that excessive myosin activity shifts the furrow toward the anterior of the embryo. Our work thus demonstrates that the regulation of asymmetrically localized myosin is critical to ensure that the positions of the furrow and of the spindle midzone coincide throughout cytokinesis.

Results

PAR-4 and CUL-5 are required to coordinate spindle and furrow positions

cullin-5 (*cul-5*) deletion mutants are viable and do not display obvious defects during embryonic development; however, they enhance embryonic lethality caused by weak *cul-2* depletion (Sasagawa et al., 2007), indicating that CUL-5 plays a role, albeit nonessential on its own, during embryonic development. To decipher the role of CUL-5, we tested possible genetic interactions with different *par* mutants and found that the loss of CUL-5 strongly enhances *par-4* mutant defects. *cul-5(ok1706)* embryos have a very low embryonic lethality and *par-4(RNAi)* or *par-4(it47)* thermosensitive embryos grown at permissive temperature (15°C) show 27% and 56% embryonic lethality, respectively. *cul-5(ok1706) par-4(RNAi)* and *cul-5(ok1706) par-4(it47)* double mutant embryos show stronger embryonic lethality, at 67% and 95%, respectively (Fig. S1 A). We next recorded the first division of *cul-5(ok1706) par-4(it47)* embryos by differential interference contrast (DIC) microscopy at semi-permissive temperature (20°C) and measured the position of the furrow once it spanned the entire embryo. Like wild-type embryos, single *cul-5(ok1706)* mutants divide asymmetrically (Fig.1, A and B; and Video 1). In *par-4(it47)* single mutants the cytokinetic furrow is slightly shifted toward the anterior (Fig.1, A and B; and Video 1). The furrow is localized further toward the anterior in *cul-5(ok1706) par-4(it47)* double mutants (Fig.1, A and B; and Video 1). Similar results were obtained at restrictive temperature (25°C; unpublished data) and upon *par-4* RNAi (Fig. S1 C). Thus, both CUL-5 and PAR-4 are involved in regulating the position of the cytokinetic furrow during asymmetric cell division.

We also found that the loss of the RING-containing protein RBX-2, which associates with CUL-5 in ubiquitine ligase complexes (Kamura et al., 2004), increases the embryonic lethality of *par-4(RNAi)* and *par-4(it47)* embryos (Fig. S1 B). Moreover, whereas *rbx-2(ok1617)* mutants divide asymmetrically, the cytokinetic furrow is shifted toward the anterior in *rbx-2(ok1617); par-4(it47)* and *rbx-2(ok1617); par-4(RNAi)* embryos, similar to *cul-5(ok1706) par-4(it47)* and *cul-5(ok1706) par-4(RNAi)* embryos (Fig. 1, A and B; Video 1; and Fig. S1 C). These results suggest that CUL-5 and RBX-2 may function in the same ubiquitin ligase complex to regulate cytokinetic furrow position.

To test whether the furrow position defects of *cul-5(ok1706) par-4(it47)* embryos were a result of the mispositioning of the mitotic spindle along the anteroposterior axis of the embryo, we measured the position of the spindle at the onset of cytokinesis in strains expressing an α-tubulin::YFP (α-tub::YFP) transgene. Surprisingly, we found the spindle to be correctly located toward the posterior pole in *α-tub::YFP; cul-5(ok1706) par-4(it47)* embryos, similar to *α-tub::YFP*, *α-tub::YFP; cul-5(ok1706)*, and *α-tub::YFP*; *par-4(it47)* embryos (Fig. 1 C). Furthermore, both in wild-type and *cul-5(ok1706) par-4(it47)* embryos, the spindle appears symmetrical, with the midzone localized centrally and the two sets of chromosomes distributed at equal distance from the midzone during anaphase (Fig. 1 D). Altogether, our results show that furrow mispositioning in *cul-5(ok1706) par-4(it47)* embryos is not caused by defects in spindle position or general organization.

To compare spindle and furrow positions, we measured the distance between the anterior spindle aster and the furrow during ingression and compared it to spindle length (Fig. 1 F, inset). In *α-tub::YFP* and *α-tub::YFP; cul-5(ok1706)* embryos, the anterior aster-furrow distance is close to 50% of spindle length, indicating that furrow position correlates with the spindle center (Fig. 1, E and F; and Video 2). In *α-tub::YFP*; *par-4(it47)* embryos, the anterior aster-furrow distance is slightly shorter. It is further decreased in *α-tub::YFP; cul-5(ok1706) par-4(it47)* embryos (Fig. 1, E and F; and Video 2), showing that the furrow is shifted toward the anterior compared with the spindle center. Thus the position of the cytokinetic furrow does not coincide with the spindle center in *cul-5(ok1706) par-4(it47)* mutants, a phenotype that to our knowledge has never been described thus far.

Furrow mispositioning is not caused by defects in the centralspindlin or astral microtubule pathway

Two redundant pathways, depending on centralspindlin and astral microtubules, induce cytokinesis in the early *C. elegans* embryo (Dechant and Glotzer, 2003). We tested whether either of these pathways was affected in *cul-5(ok1706) par-4(it47)* embryos. Inactivation of the centralspindlin protein ZEN-4/MKLP1 does not prevent furrow ingression but leads to furrow regression during the late steps of cytokinesis (Raich et al., 1998; Fig. 2 A). *cul-5(ok1706) par-4(it47)* mutants undergo complete cytokinesis (Fig. 2 A), suggesting that the centralspindlin pathway is functional in these embryos. To

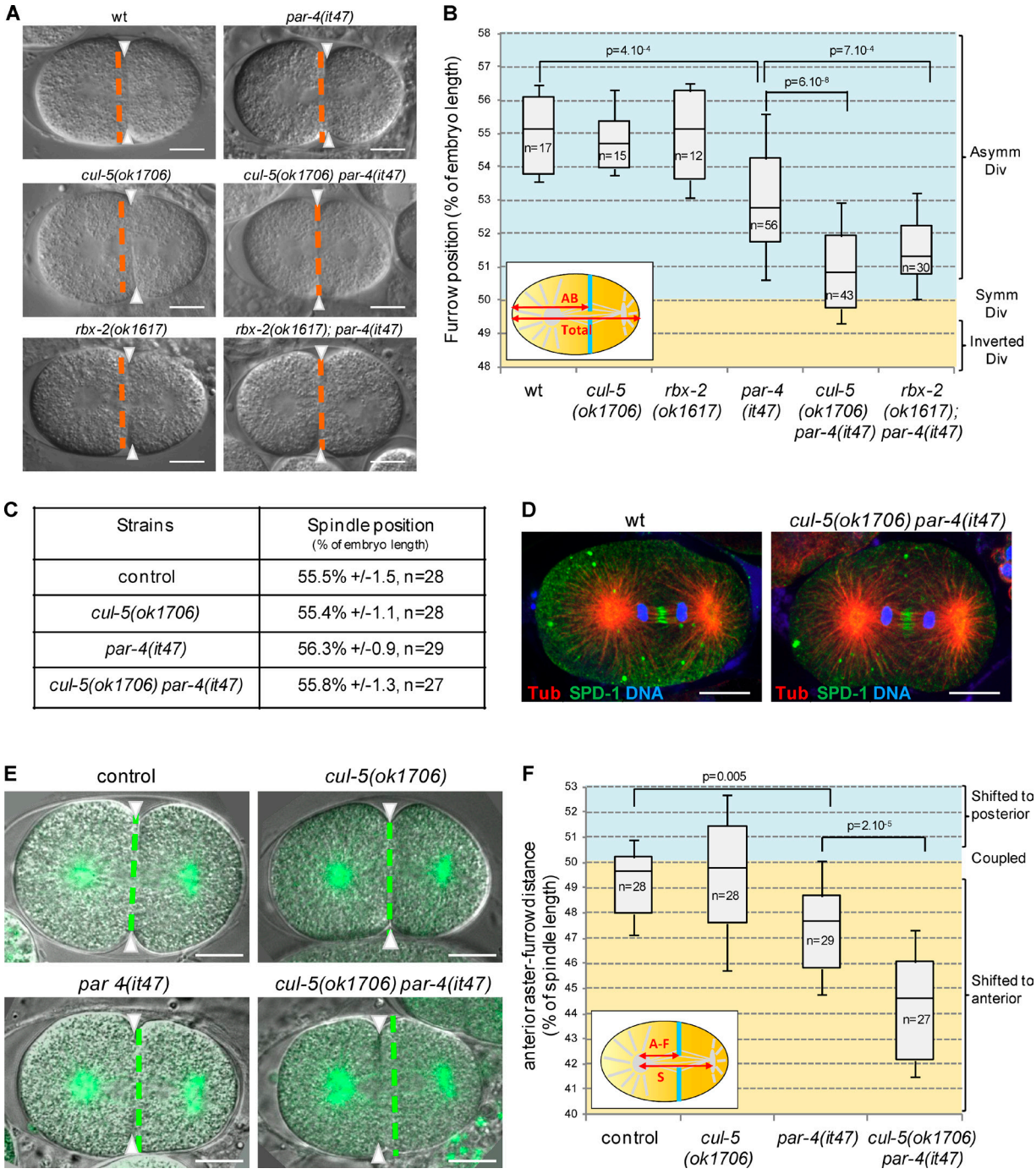

Figure 1. **CUL-5/RBX-2 and PAR-4 regulate cytokinetic furrow position.** (A and B) The furrow is shifted toward the anterior in *cul-5(ok1706) par-4(it47)* and *rbx-2(ok1617); par-4(it47)* embryos. DIC images (A) and quantification of furrow position (B) in dividing one-cell embryos of the indicated genotypes. Furrow position was measured when the furrow spanned the entire embryo. Orange dashed lines correspond to the embryo center and arrowheads to furrow position. As depicted in the inset (B), furrow position is the distance between the anterior pole and the furrow (AB size) expressed as a percentage of total embryo length (0% corresponds to the anterior pole, 100% to the posterior pole). See also Fig. S1 and Video 1. (C) Position of the spindle center at the onset of cytokinesis in one-cell embryos of the indicated genotypes (all strains also express an α-tub::YFP transgene). (D) Localization of the spindle midzone protein SPD-1 and of DNA during anaphase is normal in *cul-5(ok1706) par-4(it47)* embryos. Confocal section of wild-type and *cul-5(ok1706) par-4(it47)* one-cell anaphase embryos stained for α-tubulin (red), SPD-1 (green), and DNA (blue). More than 10 anaphase embryos per genotype were observed and representative images are shown. (E and F) Furrow and spindle positions are uncoupled in *cul-5(ok1706) par-4(it47)* embryos. Superposed confocal sections and DIC images (E) and quantification of furrow/spindle coupling (F) in dividing one-cell embryos of the indicated genotypes (all strains also express an α-tub::YFP transgene [green]). Green dashed lines correspond to the spindle center and arrowheads to furrow position. As depicted in the inset (F), the distance between the anterior aster and the furrow (A-F) was measured during ingression and expressed as a percentage of spindle length (50% corresponds to the furrow position being coupled with spindle center, below 50% corresponds to a shift of the furrow toward the anterior, and above 50% corresponds to a shift toward the posterior). See also Video 2.In all images, embryos are oriented with the anterior to the left. Bars, 10 µm. P-values from Student's *t* test.

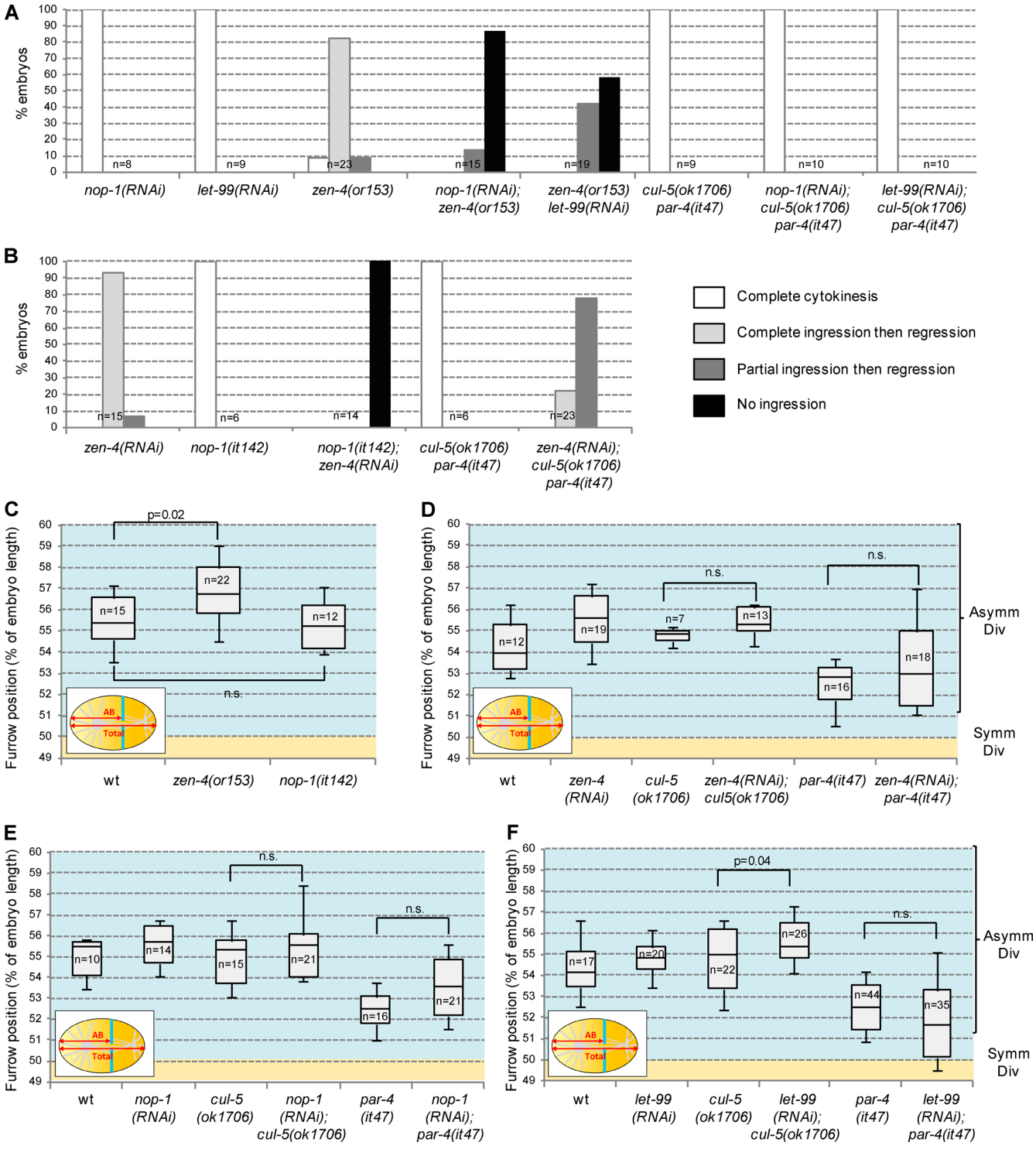

Figure 2. **Inhibition of centralspindlin or astral microtubule pathway does not account for furrow mispositioning.** (A) Inactivation of the astral microtubule pathway by *nop-1* and *let-99* RNAi does not inhibit furrow ingression in *cul-5(ok1706) par-4(it47)* one-cell embryos. *nop-1* and *let-99* RNAi effectively inhibited astral microtubule signaling as judged by their ability to inhibit furrow ingression in *zen-4(or153)* mutant. (B) Inactivation of the centralspindlin pathway by *zen-4* RNAi partially inhibits furrow ingression in *cul-5(ok1706) par-4(it47)* one-cell embryos. *zen-4* RNAi effectively inhibited centralspindlin signaling as the furrow regresses in *zen-4(RNAi)* embryos and does not ingress in *nop-1(it142); zen-4(RNAi)* embryos. (C–F) Inactivation of centralspindlin or the astral microtubule pathway does not shift the furrow toward the anterior. Furrow position was measured in *zen-4(or153)* and *nop-1(it142)* mutants (C) and in wild-type, *cul-5(ok1706)*, or *par-4(it47)* embryos treated with *zen-4* (D), *nop-1* (E), *or let-99* (F) RNAi. Furrow position was measured when the furrow spanned the entire embryo. P-values from Student's *t* test.

uncover possible subtle defects in this pathway, we tested whether inactivating the astral microtubule pathway in *cul-5(ok1706) par-4(it47)* embryos leads to cytokinesis defects. Indeed, inactivating astral microtubule signaling by depleting the serine-rich protein NOP-1 or the DEP domain protein LET-99, for instance, does not prevent cytokinesis on its

own but blocks furrow ingression when centralspindlin signaling is also impaired (Bringmann et al., 2007; Tse et al., 2012; Fig. 2 A). However, neither *nop-1* nor *let-99(RNAi)* affects furrow ingression in *cul-5(ok1706) par-4(it47)* embryos (Fig. 2 A), showing that centralspindlin signaling is fully functional in these embryos. To test whether astral microtubule signaling is defective in *cul-5(ok1706) par-4(it47)* mutants, we performed the inverse experiment. Inactivating centralspindlin using *zen-4* RNAi leads to complete furrow ingression followed by regression in a wild-type background and completely inhibits furrow ingression in embryos with inactive astral microtubule signaling (*nop-1(it142)* mutants; Tse et al., 2012; Fig. 2 B). When *zen-4* RNAi was performed in *cul-5(ok1706) par-4(it47)*, the furrow either ingressed completely (5/23 embryos) or partially (18/23 embryos) before regressing (Fig. 2 B). Thus the astral microtubule pathway is active in *cul-5(ok1706) par-4(it47)* embryos, albeit to a lower extent than in wild type.

We next tested whether the inactivation of centralspindlin or of the astral microtubule pathway could lead to furrow mispositioning. Centralspindlin (*zen-4(or153)*) and astral microtubule (*nop-1(it142)*) defective mutants divide asymmetrically (Severson et al., 2000; Tse et al., 2012; Fig. 2 C). Moreover, inactivation of centralspindlin (*zen-4* RNAi) or astral microtubule signaling (*nop-1* and *let-99* RNAi) in either *par-4(it47)* or *cul-5(ok1706)* single mutants does not shift the furrow toward the anterior (Fig. 2, D–F). In conclusion, although astral microtubule signaling is only partially active in *cul-5(ok1706) par-4(it47)* embryos, our data indicate that defects in either centralspindlin or astral microtubule signaling cannot account for the furrow positioning defects observed in these embryos.

PAR-4 and CUL-5 prevent cortical accumulation of ANI-2

We next sought to identify the mechanism by which PAR-4 and CUL-5 regulate furrow position. PAR-4 has been previously shown to be a negative regulator of ANI-2 (Chartier et al., 2011). ANI-2 is barely detected in wild-type one- and two-cell embryos but a weak accumulation of ANI-2 is observed at the cortex between the anterior and posterior cells in *par-4(it47)* two-cell embryos (Fig. 3, A and B; Chartier et al., 2011). We found that ANI-2 also accumulates at this cortex in *cul-5(ok1706)* embryos (Fig. 3, A and B). Furthermore, we observed a strong cortical accumulation of ANI-2 in *cul-5(ok1706) par-4(it47)* double mutants (Fig. 3, A and B). Thus PAR-4 and CUL-5 are both negative regulators of ANI-2 (see Fig. 8 E). No increase in total ANI-2 protein levels could be detected in *cul-5(ok1706) par-4(it47)* embryonic extracts (Fig. S1 D), suggesting that CUL-5 and PAR-4 may not regulate the global stability of ANI-2 but rather its accumulation at the cortex.

To determine whether ANI-2 is responsible for furrow mispositioning in *cul-5(ok1706) par-4(it47)* embryos, we tested whether ANI-2 depletion can restore normal furrow position in those embryos. *ani-2(RNAi)* does not lead to changes in furrow position on its own but furrows are localized more posteriorly in *ani-2(RNAi); cul-5(ok1706) par-4(it47)* embryos than in *cul-5(ok1706) par-4(it47)* embryos (Fig. 3 C). *ani-2(RNAi)* thus rescues the defects of *cul-5(ok1706) par-4(it47)* embryos, indicating that ANI-2 contributes to furrow mispositioning in *cul-5(ok1706) par-4(it47)* embryos.

PAR-4 and ANI-1 both regulate furrow position

Previous work suggested that ANI-2 is a negative regulator of ANI-1 (Amini et al., 2014). Cortical accumulation of ANI-2 in *cul-5(ok1706) par-4(it47)* embryos raises the possibility that ANI-1 may be inhibited in those embryos. However, consistent with a previous study (Maddox et al., 2005), we find that *ani-1* depletion alone does not shift the furrow toward the anterior (Fig. 4, A and B; and Video 3). Thus inhibition of ANI-1 is not sufficient to explain furrow mispositioning in *cul-5(ok1706) par-4(it47)* embryos. We therefore hypothesized that *par-4* and/or *cul-5* might regulate furrow position not only via the regulation of anillins but also via an anillin-independent pathway. To test this hypothesis, we depleted ANI-1 in *cul-5(ok1706)* and in *par-4(it47)* single mutant embryos grown at 20°C. Although *ani-1(RNAi)* does not change furrow position in *cul-5(ok1706)* mutants, we observed strong furrow mispositioning in *ani-1(RNAi); par-4(it47)* embryos (Fig. 4, A and B; and Video 3). In most embryos, the furrow was even observed in the anterior half of the embryo. Similar results were obtained when ANI-1 was depleted in another *par-4* mutant, *par-4(it57)* (Fig. S2 A).

In *α-tub::YFP*; *ani-1(RNAi)*; *par-4(it47)* embryos the spindle center is located toward the posterior pole, similar to *α-tub::YFP*, *α-tub::YFP*; *ani-1(RNAi)*, and *α-tub::YFP*; *par-4(it47)* embryos (Fig. 4 C). Furthermore, the anterior aster-furrow distance is dramatically decreased in *α-tub::YFP; ani-1(RNAi)*; *par-4(it47)* compared with control and single mutant embryos (Fig. 4, D and E; and Video 4). An even stronger effect is observed when worms are grown at fully restrictive temperature for *par-4(it47)* (25°C; Fig. S2 B). The cytokinetic furrow is therefore strongly shifted toward the anterior and away from the spindle center in *ani-1(RNAi)*; *par-4(it47)* embryos. In the most severe cases, the furrow was displaced to such an extent that it could not properly segregate DNA (Fig. S2 C). Our results led us to propose that PAR-4 controls furrow position by regulating ANI-2 and ANI-1 together with CUL-5 but also by acting in an anillin-independent pathway (see Fig. 8 E). Strong furrow mispositioning is observed when these two pathways are simultaneously inhibited. Consistent with our hypothesis that ANI-2 acts upstream of ANI-1, we find that ANI-2 depletion does not suppress defects of *ani-1(RNAi); par-4(it47)* embryos (Fig. S2 D).

PIG-1 and ANI-1 both regulate furrow position

We next searched for PAR-4 targets that could be involved in the anillin-independent pathway. PAR-4 phosphorylates and activates AMPK-related kinases (Lizcano et al., 2004). Two of these kinases have been implicated in asymmetric cell division: PAR-1, which regulates several aspects of asymmetric division in early embryos (Kemphues et al., 1988; Tenlen et al., 2008; Benkemoun et al., 2014), and PIG-1, the homologue of vertebrate MELK, a kinase regulating cytokinesis in *Xenopus laevis* embryos (Le Page et al., 2011). In *C. elegans*, both PIG-1 and PAR-4 regulate neuroblast asymmetric division (Cordes et al., 2006; Ou et al., 2010; Chien et al., 2013) and *pig-1* mutants enhance the polarity defects of weak *par-2* mutants in two-cell embryos (Morton et al., 2012). PIG-1 is expressed in embryos (Fig. 5 A) where the endogenous protein is localized in the cytoplasm and at the cortex between adjacent cells (Fig. 5, B–G). Time-lapse imaging of embryos expressing

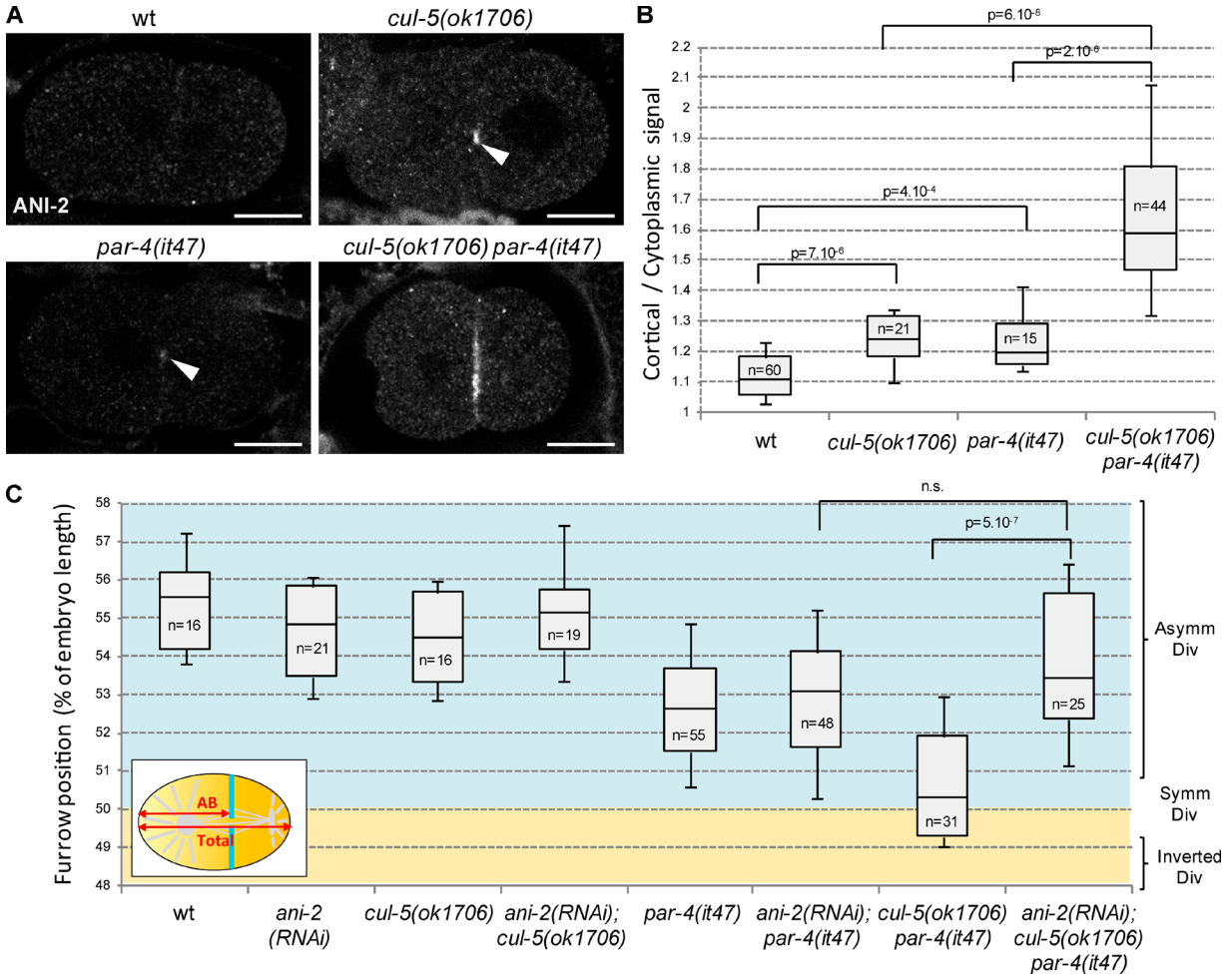

Figure 3. **ANI-2 accumulates and is required to misposition the furrow in *cul-5 par-4* embryos.** (A and B) ANI-2 strongly accumulates at the cortex between AB and P1 in *cul-5(ok1706) par-4(it47)* embryos. Confocal sections of two-cell embryos (A) of the indicated genotypes stained with anti-ANI-2 antibody and quantification (B) of ANI-2 cortical accumulation (see Materials and methods for details). Most wild-type embryos show no ANI-2 staining. ANI-2 weakly accumulates in *cul-5(ok1706)* and *par-4(it47)* embryos (arrowheads) and strongly in *cul-5(ok1706) par-4(it47)* embryos. Bars, 10 µm. See also Fig. S1 D. (C) *ani-2* RNAi suppresses furrow position defects of *cul-5(ok1706) par-4(it47)* embryos. Furrow position was measured when the furrow spanned the entire embryo. P-values from Student's *t* test.

a GFP::PIG-1 transgene shows that cortical recruitment occurs during mitosis (Video 5).

To determine whether PAR-1 or PIG-1 were involved in the ANI-1–independent pathway, we analyzed furrow position in embryos lacking ANI-1 and either PAR-1 or PIG-1. In *ani-1(RNAi); par-1(zu310)* embryos, the furrow is not shifted toward the anterior (Fig. S3 A). In contrast, although *pig-1(gm344)* embryos divide as wild type, *ani-1(RNAi); pig-1(gm344)* embryos behave similarly to *ani-1(RNAi); par-4(it47)* embryos: their furrows are located in the anterior half of the embryo (Fig. 5, H and I) and strongly shifted away from the spindle center (Fig. 5 J). This furrow mispositioning can lead to defects in DNA segregation (Fig. 5 K). Thus PIG-1 and ANI-1 both regulate furrow position and PIG-1 is likely to be a PAR-4 target in the anillin-independent pathway (see Fig. 8 E). Consistent with this model, *pig-1(gm344); par-4(it47)* embryos show only mild furrow position defects, similar to *par-4(it47)* embryos (Fig. S 3B). Finally, *pig-1(gm344); cul-5(ok1706)* embryos do not have furrow position defects (Fig. S3 C) and ANI-2 localization is not affected in *pig-1(gm344)* embryos (Fig. S3 D), suggesting that PIG-1 is not involved in regulating the anillin-dependent pathway.

PAR-4 and ANI-1 are required to maintain furrow position throughout cytokinesis

To determine the dynamics of the strong furrow mispositioning observed in *ani-1(RNAi)*; *par-4(it47)* embryos, we followed the position of the furrow during ingression by visualizing it with an NMY-2::GFP transgene. In both control and *ani-1(RNAi)* embryos, furrow ingression initiates between 50% and 60% embryo length, in the vicinity of the spindle midzone (Fig. 6, A and C). The furrow then ingresses without major changes in its position (Fig. 6, A′, A″, and C; and Video 6). In *par-4(it47)* embryos, the furrow initiates between 50% and 60% embryo length and is then weakly displaced toward the anterior (Fig. 6 C). Most *ani-1(RNAi)*; *par-4(it47)* embryos (18/21) initiate furrowing in the vicinity of the spindle midzone (Fig. 6, B and C). This is followed by a strong shift toward the anterior (Fig. 6, B′ and C; and Video 6). In 3/21 embryos, we observed that furrow ingression does not occur perpendicularly to the anteroposterior axis, one furrow tip starting ingression very close to the posterior pole and another very close to the anterior pole. Both furrow tips then move simultaneously

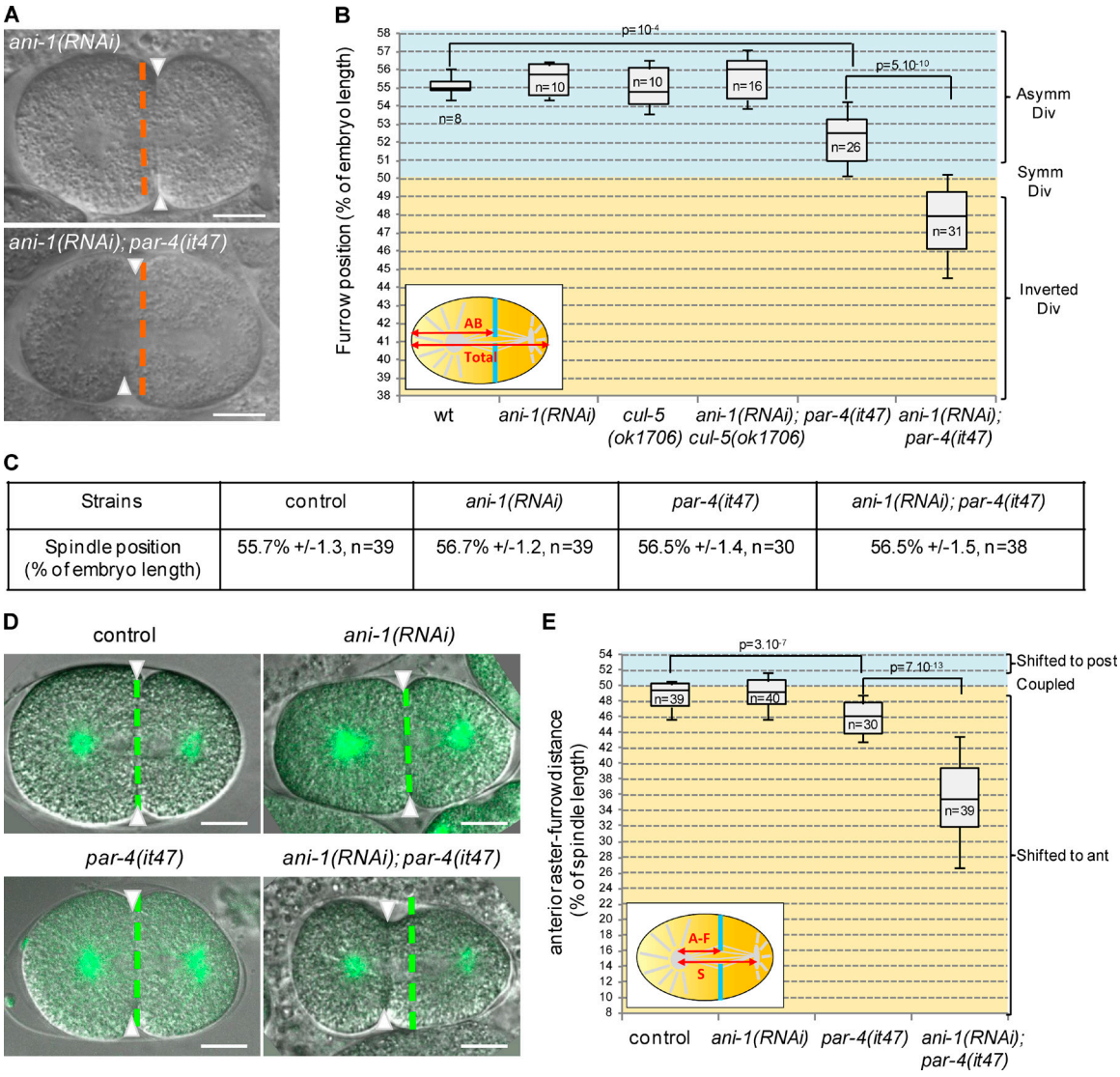

Figure 4. **Loss of PAR-4 and ANI-1 leads to strong furrow mispositioning.** (A and B) *ani-1(RNAi); par-4(it47)* embryos show strong furrow mispositioning. DIC images (A) and quantification of furrow position (B) in dividing one-cell embryos of the indicated genotypes. Furrow position was measured when the furrow reached its most anterior position. Orange dashed lines correspond to the embryo center and arrowheads to furrow position. See also Fig. S2 (A and D) and Video 3. (C) Position of the spindle center at the onset of cytokinesis in one-cell embryos of the indicated genotypes (all strains also express an α-tub::YFP transgene). (D and E) Furrow and spindle positions are strongly uncoupled in *ani-1(RNAi); par-4(it47)* embryos. Superposed confocal sections and DIC images (D) and quantification of furrow/spindle coupling (E) in dividing one-cell embryos of the indicated genotypes (all strains also express an α-tub::YFP transgene [green]). Furrow position was measured when the furrow reached its most anterior position. Green dashed lines correspond to the spindle center and arrowheads to furrow position. Experiment was performed at 20°C. See also Fig. S2 (B and C) and Video 4. Bars, 10 µm. P-values from Student's *t* test.

toward the center of the embryo (Fig. S4, A–A″ and B; and Video 6). Thus, the initial position of furrow ingression is essentially correct in *ani-1(RNAi)*; *par-4(it47)* embryos but PAR-4 and ANI-1 are then essential to maintain furrow position during ingression.

Notably, in 13/21 *ani-1(RNAi)*; *par-4(it47)* embryos, the furrow moves so far toward the anterior that both sets of chromosomes are initially located on its posterior side (Fig. 6 B′ and Video 6). However, at the end of cytokinesis the furrow is slightly displaced toward the posterior whereas the DNA moves toward the anterior. As a result, the anterior set of chromosomes goes through the furrow before its final closure, allowing proper DNA segregation (Fig. 6, B″ and C; and Video 6).

PAR-4 and ANI-1 regulate furrow position in other asymmetrically dividing cells

Strikingly, furrow mispositioning in *ani-1(RNAi); par-4(it47)* embryos always occurs toward the anterior side of the embryo, suggesting that this may be linked to the inherent asymmetry of the one-cell embryo. We tested whether defects in furrow positioning are specific to asymmetrically dividing cells by observing two-cell stage embryos in which the anterior AB cell normally divides symmetrically and the posterior P1 cell divides asymmetrically (Fig. S5 A). In *ani-1(RNAi); par-4(it47)* two-cell embryos, the furrow is shifted toward the anterior in the posterior cell (Fig. S5, A and C) whereas the symmetrically dividing anterior cell is insensitive to the absence of PAR-4 and ANI-1 (Fig. S5, A and B). This suggests that PAR-4 and

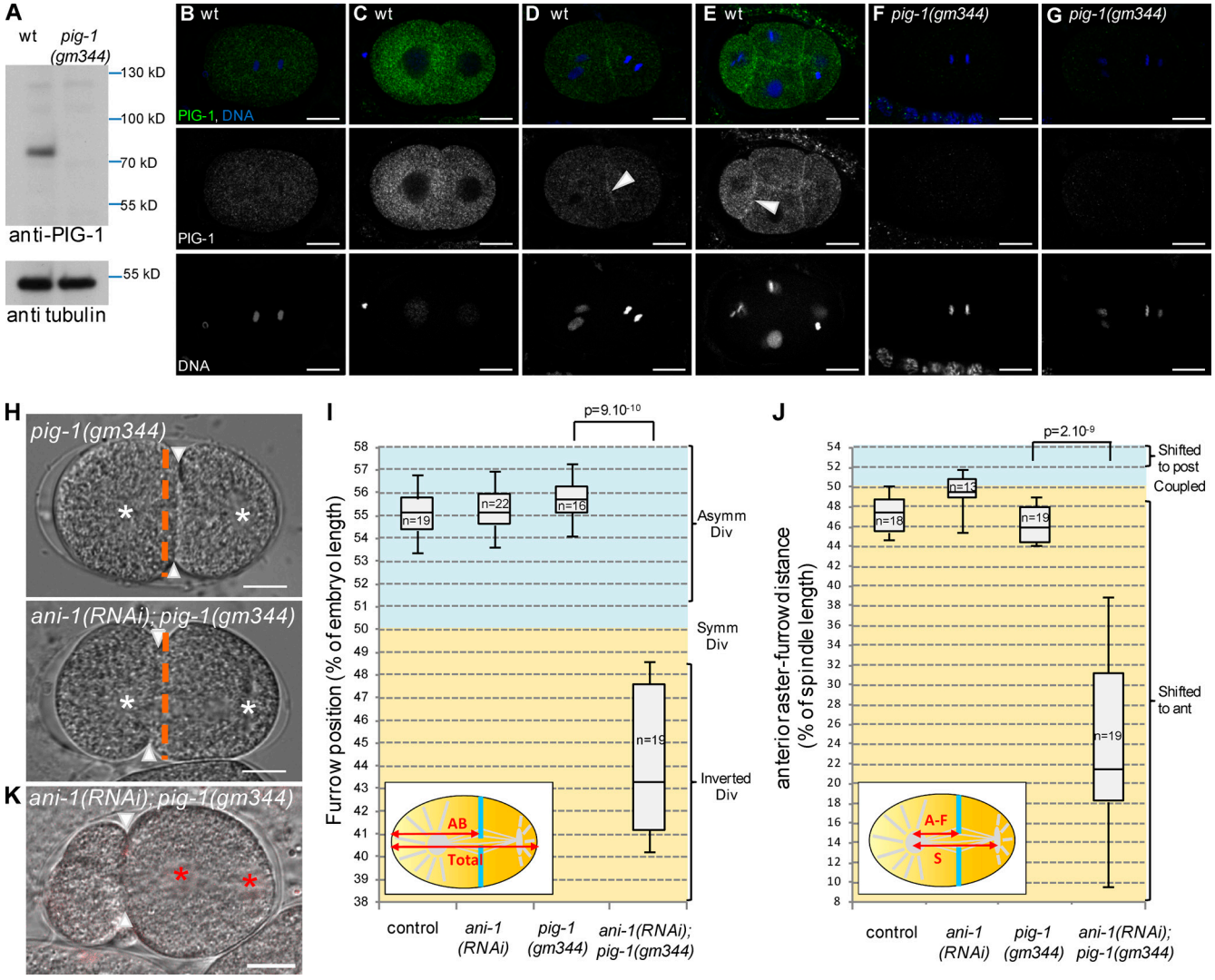

Figure 5. **Loss of PIG-1 and ANI-1 leads to strong furrow mispositioning.** (A–G) PIG-1 is expressed in embryos. Western blot (A) shows that PIG-1 is expressed in wild-type but not *pig-1(gm344)* embryonic extracts. Tubulin is used as a loading control. Immunostainings (B–G) show that PIG-1 is expressed in early wild-type (B–E) but not *pig-1(gm344)* embryos (F and G). PIG-1 is localized in the cytoplasm in one-cell (B) and early two-cell (C) embryos, it is also localized at the cortex between adjacent cells in late two-cell (D) and four-cell embryos (E). See also Video 5. (H–J) *ani-1(RNAi); pig-1(gm344)* embryos show strong furrow mispositioning. DIC images (H) and quantification of furrow position (I) and furrow/spindle coupling (J) in dividing one-cell embryos of the indicated genotypes. In J, all strains also express an α-tub::YFP transgene. Furrow position was measured when the furrow reached its most anterior position. (H) Orange dashed lines correspond to the embryo center, arrowheads to furrow position, and white asterisks to spindle asters. See also Fig. S3. (K) Strong furrow mispositioning can lead to DNA segregation defects in *ani-1(RNAi); pig-1(gm344)* embryos. DIC pictures of an *ani-1(RNAi); pig-1(gm344)* embryo in which all DNA is inherited by the posterior cell. This embryo also expressed an mCherry::HIS-58 transgene to monitor DNA position (red asterisks). Arrowheads indicate furrow position. 12 out of 28 embryos showed this DNA segregation phenotype. Bars, 10 µm. P-values from Student's *t* test.

ANI-1 may regulate furrow position specifically in asymmetrically dividing cells.

Myosin abnormally accumulates at the anterior cortex of *ani-1; par-4* and *ani-1; pig-1* embryos

Our previous results suggest that furrow displacement is dictated by some intrinsic polarity of those cells. Considering its ability to induce cytokinesis in neuroblasts (Cabernard et al., 2010; Ou et al., 2010), myosin is a good candidate for causing the furrow to be displaced toward the anterior. We first analyzed myosin II dynamics during division using an NMY-2::GFP transgene. As previously described (Werner et al., 2007), in wild-type one-cell embryos, NMY-2::GFP localizes to the anterior cortex at metaphase, and then it briefly dissociates from the cortex and reaccumulates at the anterior cortex and in the equatorial region shortly after anaphase onset (Video 7). Myosin intensity at the anterior cortex increases after anaphase and then rapidly decreases before cytokinesis onset (Fig. 7 A and Video 7). In two-cell embryos, NMY-2::GFP also accumulates at the anterior cortex of the P1 cell before division whereas it is initially symmetrically localized in the AB cell and then removed from both poles of the cell before division (Video 8). In *ani-1(RNAi); par-4(it47)* embryos, myosin follows essentially the same pattern as in control embryos but myosin accumulation at the anterior cortex after anaphase is considerably stronger and lasts longer (Fig. 7 A and Video 7). No strong defects were observed in *ani-1(RNAi)* embryos. Consistent with previous observations (Chartier et al., 2011), myosin accumulation at the anterior cortex also lasts longer in *par-4(it47)* embryos, albeit to a lower levels than in *ani-1(RNAi); par-4(it47)*

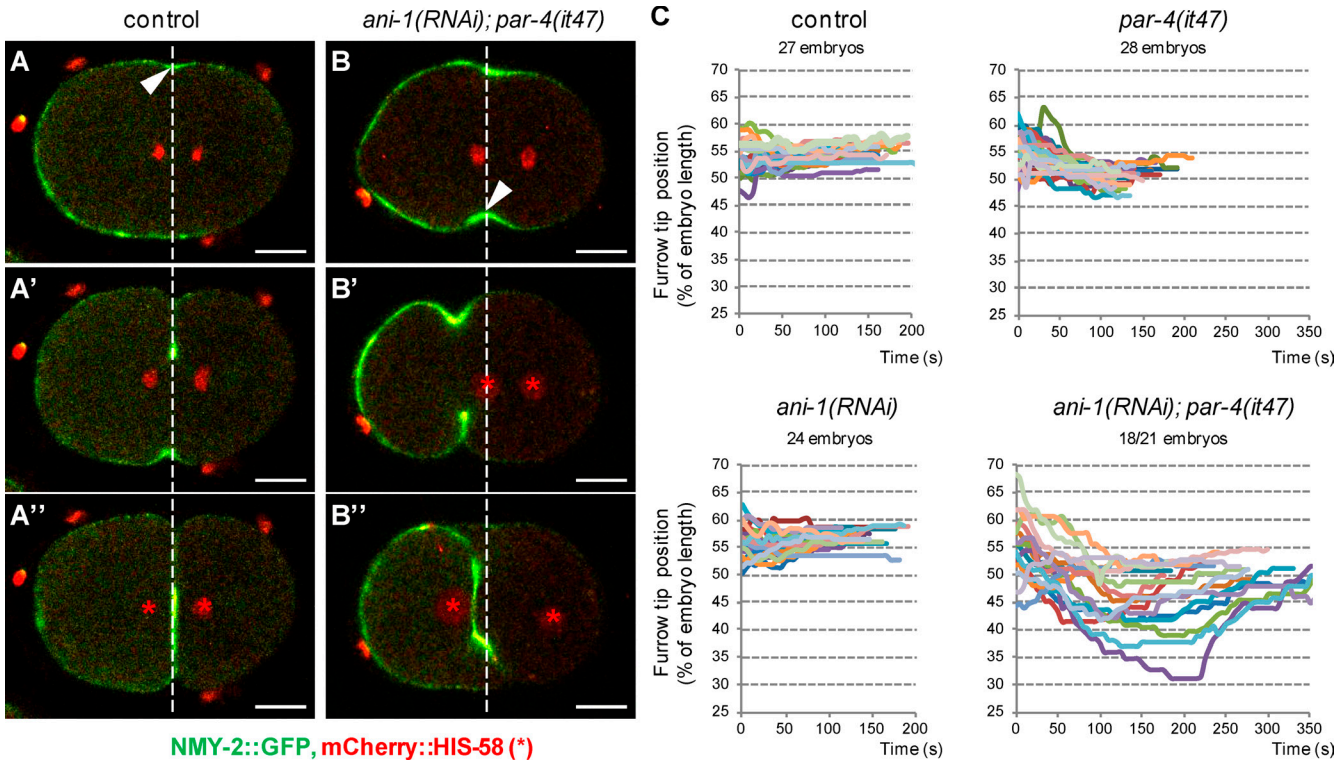

Figure 6. **Dynamics of furrow ingression in *ani-1; par-4* embryos.** (A and B) During ingression, furrow position does not change in control embryos whereas it is strongly displaced in *ani-1(RNAi); par-4(it47)* embryos. Furrow position during ingression is monitored with an NMY-2::GFP transgene (green). DNA is monitored with an mCherry::HIS-58 transgene (red and asterisks). Images were acquired at the onset of cytokinesis (A and B), during ingression (A′ and B′), and just after furrow closure (A″ and B″). Arrowheads and white dashed lines indicate the position of initial ingression. Bars, 10 µm. See also Fig. S4 (A and B) and Video 6. (C) Graphs representing the position of the furrow tip during ingression of embryos of the indicated genotypes (all strains also express an NMY-2::GFP and mCherry::HIS-58 transgene). The furrow tip on the embryo side where ingression first initiated was tracked from ingression initiation until furrow closure. Its position is expressed as a percentage of embryo length (0% corresponds to the anterior pole and 100% to the posterior pole). Each colored track corresponds to the furrow tip position of a single embryo. 18/21 *ani-1(RNAi); par-4(it47)* embryos displayed such a furrow displacement; others are represented in Fig.S4 (A and B).

embryos (Fig. 7 A). Altogether, our results show that both PAR-4 and ANI-1 regulate myosin to prevent its excessive accumulation at the anterior cortex during cytokinesis (see Fig. 8, E and F). In *pig-1(gm344)* and *ani-1(RNAi); pig-1(gm344)* embryos, changes in myosin accumulation are very similar to those observed in *par-4(it47)* and *ani-1(RNAi); par-4(it47)* embryos, respectively (Fig. 7 B). This accumulation is not caused by a global change in myosin heavy or light chain levels (Fig. 7 C), suggesting that PIG-1 and ANI-1 prevent the cortical accumulation of myosin.

We assessed whether the accumulation of cortical myosin during anaphase in *ani-1(RNAi); pig-1(gm344)* embryos corresponds to activated myosin by analyzing the localization of phosphorylated myosin light chain (P-MLC). During anaphase, P-MLC is not detected at the cortex of control embryos whereas it localizes at the cortex surrounding the spindle midzone in *ani-1(RNAi)* and *pig-1(gm344)* embryos (Fig. 7 D). In *ani-1(RNAi)*; *pig-1(gm344)* embryos, P-MLC strikingly accumulates in a broad region of the cortex: it forms a cortical band that spreads toward the anterior cortex (Fig. 7 D). Thus, together, ANI-1 and PIG-1 inhibit both the accumulation and the spreading of activated myosin along the cortex.

Myosin up-regulation leads to furrow mispositioning

We noticed that both *ani-1(RNAi); par-4(it47)* and *ani-1(RNAi); pig-1(gm344)* embryos, but not *par-4(it47)*, *pig-1(gm344)*, or *ani-1(RNAi)* embryos, show unusual cortical deformations during mitosis, in particular at 25°C (Video 9, Fig. S4 C, and not depicted). To test whether myosin activity contributes to these deformations and to the anterior displacement of the furrow observed in *ani-1(RNAi); par-4(it47)* embryos, we inactivated myosin during mitosis by using a fast-inactivated myosin thermosensitive mutant (see Material and methods for details). We found that, contrary to *α-tub::YFP; ani-1(RNAi); par-4(it47)* embryos, *α-tub::YFP nmy-2(ne1490); ani-1(RNAi); par-4(it47)* embryos do not show cortical deformations (Video 9). Moreover, the furrow position defects of *α-tub::YFP; ani-1(RNAi); par-4(it47)* embryos are rescued in *α-tub::YFP nmy-2(ne1490); ani-1(RNAi); par-4(it47)* embryos (Fig. 8, A and C). Myosin thus appears to be responsible for cortical deformations and furrow displacement in *ani-1(RNAi); par-4(it47)* embryos. Notably, when shifted to 25°C, *α-tub::YFP* control embryos also show a transient shift of the furrow toward the anterior. This shift is rescued in *α-tub::YFP nmy-2(ne1490)* embryos (Fig. 8 C) and is therefore likely caused by myosin activity. Our results show that PAR-4, PIG-1, and ANI-1 are negative regulators of myosin and that excessive myosin activity leads to cortical deformations and furrow mispositioning.

To independently confirm that an excess of myosin activity can lead to furrow mispositioning, we depleted RGA-3/4, two Rho GAPs that inhibit myosin (Schmutz et al., 2007). *rga-3/4(RNAi)* leads to anterior cortex hypercontractility during

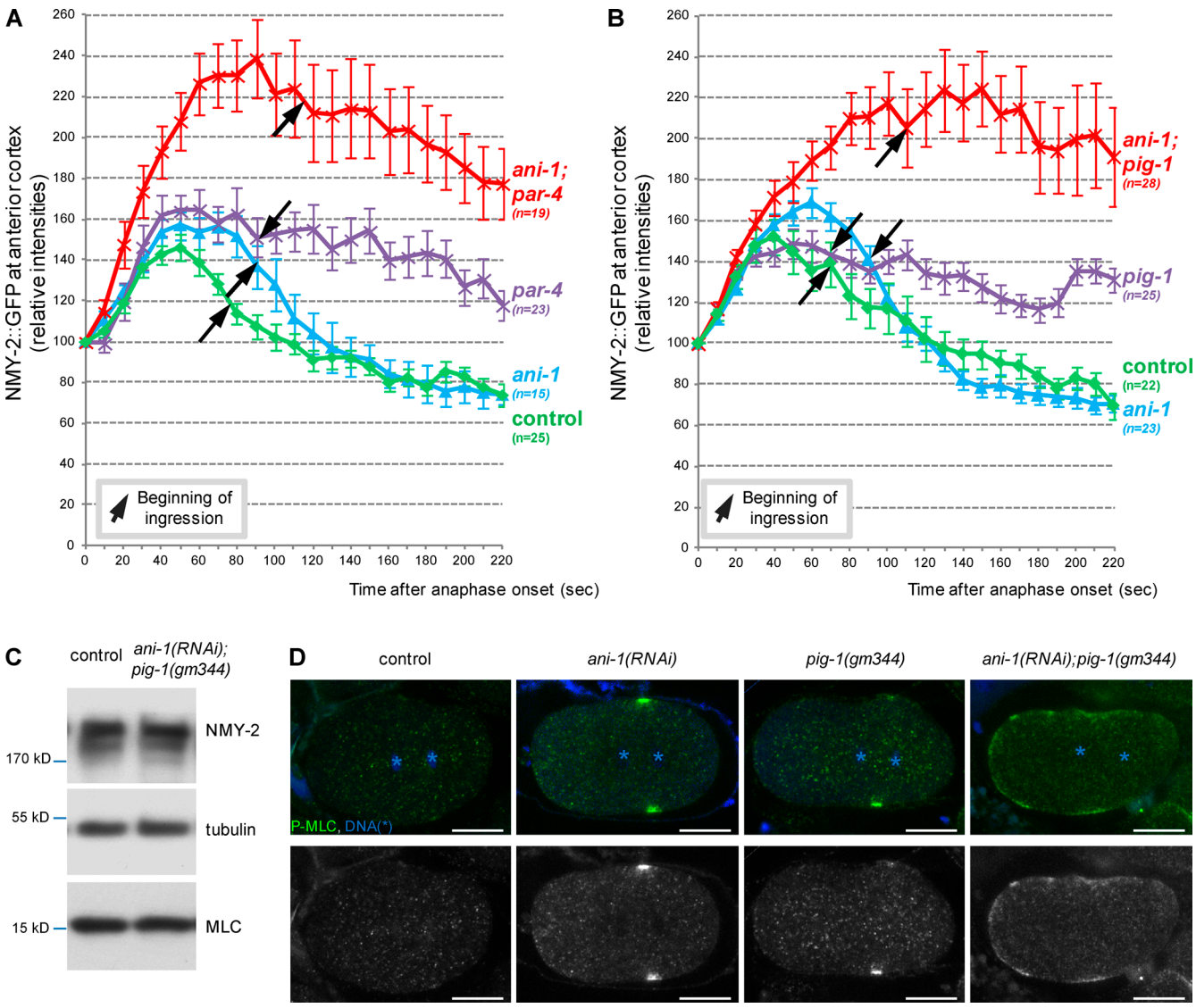

Figure 7. **Myosin is up-regulated in *ani-1; par-4* and *ani-1; pig-1* embryos.** (A and B) Myosin accumulation at the anterior cortex after anaphase onset is stronger and lasts longer in *ani-1(RNAi); par-4(it47)* (A) and *ani-1(RNAi); pig-1(gm344)* (B) embryos. Intensity of NMY-2::GFP fluorescence was measured during anaphase and cytokinesis at the anterior cortex of embryos of the indicated genotypes (all strains also express an NMY-2::GFP and mCherry::His-58 transgene) and is expressed relative to the intensity measured at anaphase onset. Arrows indicate the mean time of ingression initiation in the different strains. For examples of embryos used for quantifications, see Video 7. Error bars are SEM. (C) Western blots show that total myosin heavy and light chain levels are not affected in *ani-1(RNAi); pig-1(gm344)* embryos. Tubulin is used as a loading control. (D) At anaphase, P-MLC is not detected at the cortex of most (31/35) control embryos. It accumulates at the equatorial cortex in *ani-1(RNAi)* (24/32) and *pig-1(gm344)* (11/19) embryos and spreads along a broader cortical region in *ani-1(RNAi); pig-1(gm344)* (32/37) embryos. Asterisks indicate DNA. Bars, 10 µm.

mitosis as well as strong furrow mispositioning (Fig. 8, B and D; and Video 10). Thus, excessive myosin activity, regardless of its origin, can result in furrow displacement. Altogether our results show that the regulation of myosin is essential to prevent it from shifting the cytokinesis furrow away from the spindle midzone.

Discussion

Here we identify a novel pathway required to coordinate furrow and spindle positions during asymmetric division. This involves the regulation of anillins as well as an anillin-independent pathway (Fig. 8 E). This regulatory network prevents excessive myosin accumulation and activity at the anterior cortex. This regulation is crucial to prevent myosin from shifting the cytokinetic furrow away from the spindle midzone and is therefore essential to ensure proper DNA segregation. We propose that anterior myosin and the mitotic spindle have opposite effects on furrow position and that the final position of the furrow is the result of an equilibrium between these two opposing signals.

The major finding of our work is that the cytokinetic furrow is shifted toward the anterior in *cul-5 par-4* and *ani-1; par-4* embryos, yet their mitotic spindles are correctly localized toward the posterior pole. PAR-4, CUL-5, and ANI-1 are thus required to coordinate the position of the cytokinetic furrow with the spindle midzone. Our data show that furrowing is first induced in the vicinity of the spindle midzone, independently of the presence of PAR-4 and ANI-1. Both PAR-4 and ANI-1 are then required to maintain furrow position during ingression (Fig. 8 F). In the absence of PAR-4 and ANI-1, myosin lev-

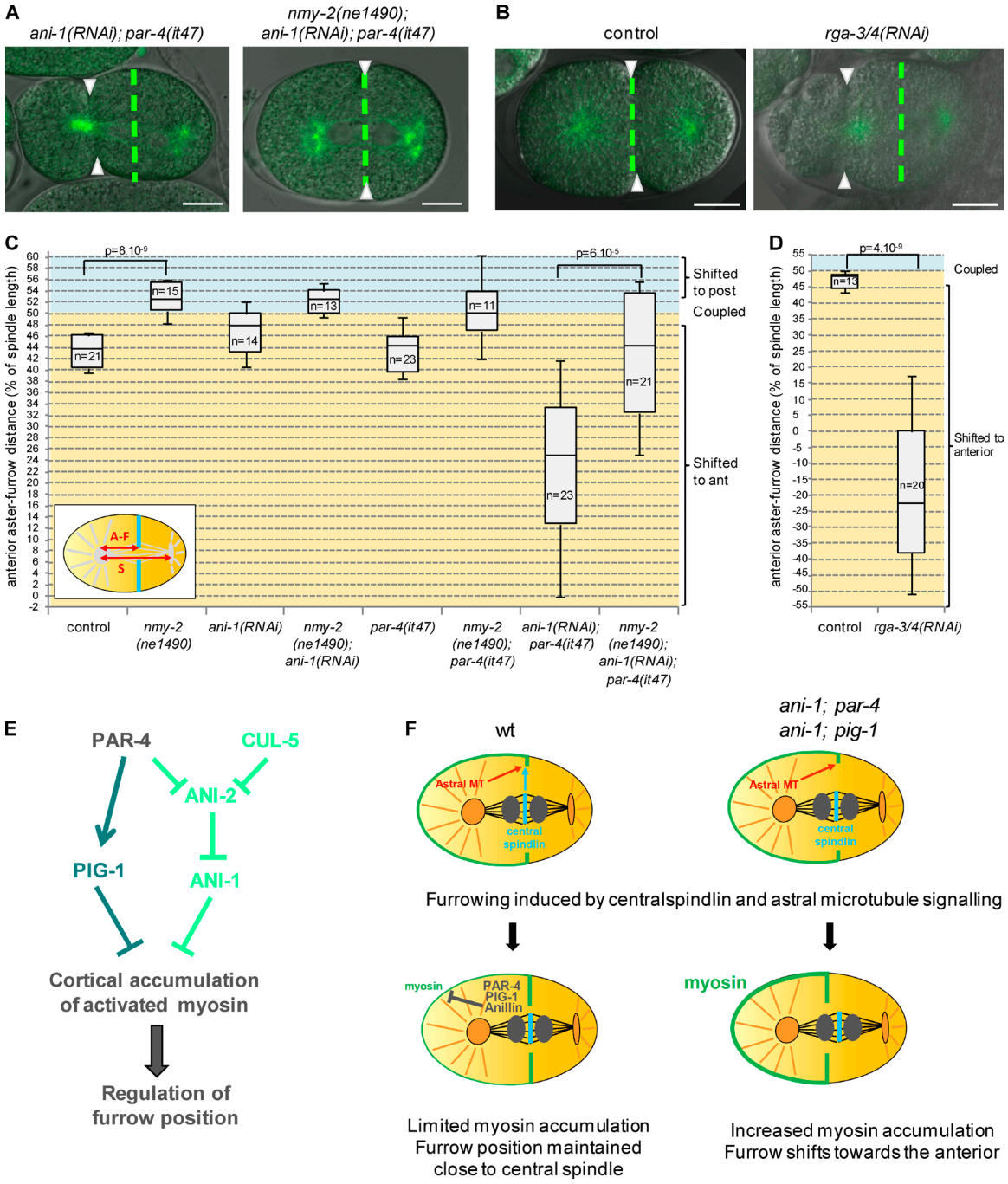

Figure 8. **Myosin up-regulation leads to furrow mispositioning.** (A–D) Furrow and spindle positions are coupled when myosin is inhibited in *ani-1(RNAi); par-4(it47)* embryos (A and C) and uncoupled when myosin is hyperactivated upon *rga-3/4(RNAi)* (B and D). Superposed confocal sections and DIC images (A and B) and quantification of furrow/spindle coupling (C and D) in dividing one-cell embryos of the indicated genotypes (all strains also express an α-tub::YFP transgene [green]). Furrow position was measured when the furrow reached its most anterior position. Green dashed lines correspond to the spindle center and arrowheads to furrow position. Bars, 10 µm. P-values from Student's *t* test. See also Videos 9 and 10. (E) A novel pathway regulating furrow positioning: PAR-4 and CUL-5 redundantly prevent ANI-2 accumulation at the cortex; ANI-2 in turns inhibits ANI-1. PAR-4 also regulates an anillin-independent pathway that involves the PIG-1/MELK kinase. Together, these two pathways prevent the cortical accumulation of activated myosin, thereby ensuring that myosin does not shift the furrow toward the anterior. (F) A model to explain furrow mispositioning in *ani-1; par-4* and *ani-1; pig-1* embryos. In wild-type as well as *ani-1; par-4* or *ani-1; pig-1* embryos, centralspindlin and astral microtubules induce furrowing in the vicinity of the spindle midzone. In wild-type embryos, PAR-4, PIG-1, and ANI-1 keep myosin accumulation and activity at the anterior cortex at a low level during cytokinesis, thereby preventing furrow displacement. In the absence of ANI-1 and PAR-4 or PIG-1, myosin accumulation at the anterior cortex increases during cytokinesis and excess of myosin activity drives the furrow toward the anterior pole of the embryo.

els are increased at the anterior cortex during cytokinesis. This leads to the displacement of the cytokinetic furrow toward the anterior (Fig. 8 F). Importantly, furrow mispositioning is also observed when anterior myosin activity is up-regulated by completely independent means, for instance by depleting the Rho GAPs RGA-3/4. Thus increased myosin activity at the anterior

cortex is sufficient to pull the furrow toward the anterior. Our results show that, like in *Drosophila* or *C. elegans* neuroblasts (Cabernard et al., 2010; Ou et al., 2010), asymmetrically localized myosin can control cytokinesis furrow position in the one-cell *C. elegans* embryo. In *Drosophila* neuroblasts myosin and the spindle are both localized on the same side of the cell and both contribute to the precise localization of the cytokinetic furrow (Roth et al., 2015). However, in the one-cell *C. elegans* embryo, anterior myosin and the posterior spindle have opposing influences on furrow position. Tight regulation of myosin is therefore crucial to maintain the equilibrium between these two effects, ensuring that the cytokinetic furrow ingresses through the spindle midzone.

Two pathways appeared to be crucial in regulating myosin: an anillin-independent pathway that regulates the cortical accumulation of myosin through the PIG-1/MELK kinase as well as an anillin-dependent pathway involving ANI-1 and ANI-2 (Fig. 8 E). PAR-4 and CUL-5 prevent the accumulation of ANI-2 at the cortex between the AB and P1 cells and regulate furrow position in an ANI-2–dependent manner. Our data suggest that CUL-5 regulates furrow position through its function in a ubiquitin ligase complex that contains the RING protein RBX-2. CUL-5 could inhibit the cortical accumulation of ANI-2 by directly promoting its degradation. However, changes in protein levels cannot be detected by Western blot analysis. This could be explained were CUL-5 only to degrade a small pool of ANI-2 locally. Alternatively, CUL-5 may degrade another factor that in turn regulates the cortical recruitment of ANI-2. Moreover, the stronger cortical accumulation of ANI-2 observed in the absence of both PAR-4 and CUL-5 indicates that ANI-2 accumulation is also regulated by PAR-4 in a CUL-5–independent manner.

Previous work (Amini et al., 2014) and our data suggest that ANI-2 inhibits ANI-1. However, furrow mispositioning defects are much more pronounced in *ani-1; par-4* embryos than in *cul-5 par-4* embryos. Inhibition of ANI-1 through the accumulation of ANI-2 in *cul-5 par-4* embryos is thus likely to be only partial. Our data show that ANI-1, together with PIG-1, inhibits both the accumulation of activated myosin and its spreading toward the anterior cortex during anaphase. One possibility is that ANI-1 and PIG-1 prevent the cortical accumulation of activated myosin by regulating its recruitment to the cortex. Alternatively they could indirectly inhibit the phosphorylation of myosin light chain. In tissue culture cells, anillin depletion leads to oscillations of the cytokinetic furrow and it has been proposed that anillin maintains the furrow in the vicinity of the spindle midzone by acting as a scaffold protein linking RhoA and MgcRacGap with actin and myosin (Piekny and Glotzer, 2008). Such a mechanism cannot account for the effect of ANI-1 on the accumulation of activated myosin. However, it could explain how ANI-1 restricts myosin localization close to the spindle midzone. ANI-1 localizes at the cortex during anaphase (Maddox et al., 2005; unpublished data) but we did not detect PIG-1 at the cortex in one-cell embryos. PIG-1 may thus regulate myosin in the cytoplasm before it is recruited to the cortex; alternatively, it may transiently interact with cortical proteins. Consistent with the latter hypothesis, PIG-1 localizes at the cortex between adjacent cells, suggesting that cell–cell contacts may stabilize its interaction with cortical proteins. Furthermore, GFP::PIG-1 appears to be recruited at the cortex at the end of mitosis, reminiscent of what happens in *Xenopus* embryos and human cells where MELK is recruited to the cortex at anaphase (Chartrain et al., 2006; Le Page et al., 2011).

PIG-1 is known to be required for the asymmetric division of both QR.p and QR.a neuroblasts (Ou et al., 2010). QR.p neuroblasts divide similarly to the one-cell embryo with their spindle being displaced toward the posterior and inducing furrowing, suggesting that PIG-1 may also coordinate spindle and furrow positions in those cells through myosin regulation. In QR.a neuroblasts, furrowing is induced by myosin accumulation at the anterior cortex and PIG-1 is required to exclude myosin from the posterior cortex (Ou et al., 2010). PIG-1 may thus regulate myosin localization in both types of asymmetric division, albeit with a different spatial pattern.

Finally, it should be noted that during the polarization phase of the embryo, both PAR-4 and ANI-1 positively regulate actomyosin contractility (Morton et al., 1992; Maddox et al., 2005; Chartier et al., 2011): contrary to what happens during anaphase, *par-4* and *ani-1* embryos show reduced pseudocleavage ingression and cortical contractility during polarity establishment. Similarly, we also observed that pseudocleavage formation is reduced in *pig-1* embryos (unpublished data). Thus, the effect of PAR-4, PIG-1, and ANI-1 on myosin depends on the stage of asymmetric cell division.

In conclusion we have identified a novel regulatory pathway that is essential to restrict the accumulation and activity of asymmetrically localized myosin and to ensure that spindle and furrow positions are coordinated. Absence of this regulation leads to a dramatic mispositioning of the cytokinetic furrow, which can impair DNA segregation. However, it is noteworthy that in some embryos late changes in furrow and DNA positions correct the initial DNA segregation defects. This suggests the existence of a supplementary control mechanism that helps to ensure proper DNA segregation. Deciphering the mechanisms that allow the correction of DNA segregation defects in the later stages of cell division will be essential to further understand how successive control mechanisms ensure robust DNA segregation during cell division.

Materials and methods

Worm strains and RNAi

Because many of our strains carry thermosensitive mutations, they were maintained at 15°C using standard procedures. A list of strains used is provided in Table S1. A strain expressing GFP::PIG-1 under the control of the *pie-1* promoter was obtained by biolistic bombardment of DP38 worms with pID3.01B-*pig-1* (*pig-1* cDNA cloned into pID3.01B; D'Agostino et al., 2006) under the control of the *pie-1* promoter and fused at the N terminus with GFP).

RNAi was performed by feeding worms with RNAi clones from the Ahringer-Source BioScience library (Kamath et al., 2003) on plates containing 1 or 3 mM IPTG. L4440 was used as a control in all RNAi experiments. For *rga-3/4* RNAi, the RNAi clone used is primarily directed against K09H11.3 (*rga-3*) but also targets Y75B7AL.4 (*rga-4*) (Schmutz et al., 2007). Double *ani-2/ani-1* RNAi was performed by growing *ani-2* and *ani-1* feeding clones separately in liquid cultures. Liquid cultures were then mixed before seeding 3 mM IPTG plates. In this experiment, *ani-2* and *ani-1* "single" RNAi was performed by diluting *ani-2* or *ani-1* clones together with the L4440 control RNAi. Conditions used for each experiment are detailed in Table S2.

Lethality tests (related to Fig. S1)

par-4(RNAi) in *cul-5(ok1706)* was performed by feeding worms on plates containing 3 mM IPTG for 24 h at 25°C before isolating a few

adults on counting plates. Adults were left to lay eggs 16–18 h before being removed from plates. *par-4(RNAi)* in *rbx-2(ok1617)* mutants was performed by feeding worms on plates containing 1 mM IPTG for 24 h at 25°C before isolating adults on counting plates. Adults were left to lay eggs 6–8 h before being removed from plates. In both cases, embryonic lethality was assessed 24 h after removing adult worms from plates, dividing the number of unhatched embryos by the total number of progeny. *cul-5(ok1706) par-4(it47)* and *rbx-2(ok1617); par-4(it47)* adults were left to lay eggs for 24 h at 15°C on OP50 plates before being removed from plates. Embryonic lethality was assessed 32–48 h after removing adult worms from plates. In each independent experiment, two to four plates were counted for each genotype. On all graphs, lethality is the mean of at least five independent experiments (more than 200 progeny were counted for each experiment).

Immunostainings

Embryos were fixed in methanol and stained according to standard procedures using rabbit anti–SPD-1 (1/50; Verbrugghe and White, 2004; provided by R. Chan, University of Michigan, Ann Arbor, MI), mouse anti-tubulin (1/1,000; DM1A; Sigma-Aldrich), rabbit anti–ANI-2 (1/1,000; residues 890–1015; Maddox et al., 2005; provided by A. Maddox, University of North Carolina, Chapel Hill, NC), rabbit anti-phospho (ser19) myosin light chain (1/30; Cell Signaling Technology), and rabbit anti–PIG-1 (1/100; this study) primary antibodies. A polyclonal anti–PIG-1 antibody was obtained after rabbit immunization with the synthetic peptide VKDNDKENASTGKNY. Immune sera were then affinity purified using the same peptide (Eurogentec). Secondary antibodies were conjugated with Alexa Fluor 488 or 568 (1/500; Invitrogen) and DNA was stained using Topro 3 (1/500; Life technologies). Observations were performed using a SPE or SP5 confocal microscope (Leica) equipped with a 63× objective (HCX Plan Apochromat, NA 1.4; Leica). Images were acquired with the LAS AF software and assembled for illustration using ImageJ and Photoshop (Adobe). Conditions used for each experiment are detailed in Table S2.

Time-lapse recordings

Embryos were mounted on 2% agarose pads in a drop of M9 medium and recordings were performed in a room maintained at 20°C or 25°C (see Table S2 for details). For experiments with *α-tubulin::YFP nmy-2(ne1490); ani-1(RNAi); par-4(it47)* embryos, worms were grown on RNAi plates at 20°C, dissected, and quickly shifted to 25°C for microscopy. Embryos that were undergoing mitosis during the temperature shift were recorded. Many embryos carrying the *nmy-2(ne1490)* mutation did not have cytokinetic furrow ingression but some still displayed at least partial furrow ingression. In a few cases, embryos had a centrally positioned spindle; those embryos were not included in the quantifications of aster/furrow distance.

DIC recordings were performed on an SPE confocal microscope equipped with a 63× objective (HCX Plan Apochromat, NA 1.4; Leica) and a charged couple device camera (DFC 360FX; Leica). Confocal and superposed confocal/DIC images were acquired on SPE or SP5 confocal microscopes with a 63× objective (HCX Plan Apochromat, NA 1.4; Leica). Images were acquired with the LAS AF software at 5-s intervals, except for Video 5 (20-s intervals), and assembled for illustration using ImageJ and Photoshop.

Image analysis and quantifications

AB size and anterior aster-furrow distance were measured using ImageJ software. The presence of the polar body was used to orient the embryos along the anteroposterior axis. Position of the furrow tip during ingression was tracked manually in ImageJ. When the two furrow tips on each side of the embryo had very close positions along the anteroposterior axis, only the first ingressing tip was tracked (Fig. 6, A–C).

Quantifications of ANI-2 (Figs. 3 B and S3 D) and myosin (Fig. 7, A and B) intensities were performed using ImageJ. For ANI-2, z-stacks were acquired (500-nm z-step) and the signal intensities of the brightest nine z-sections were summed; a 5-pixel-wide line was then drawn along the cortex separating AB and P1 and integrated density of the signal along this line was measured (cortical signal). This line was then moved to the adjacent cytoplasm and signal integrated density was measured (cytoplasmic signal). The accumulation of ANI-2 at the cortex was then expressed as the ratio between cortical and cytoplasmic signals. For myosin, a region corresponding to the most anterior 10–15% of the embryo cortex was defined and NMY-2::GFP cortical intensity was measured in a central confocal plane from anaphase onset to cytokinesis ring closure.

In all box plots, the box corresponds to the 25th to 75th percentile, the lower whisker to the first decile and the upper whisker to the ninth decile of the embryo population. The bar in the middle of the box corresponds to the median.

Worm extracts and Western blots

To analyze ANI-2 levels and PIG-1 expression, N2, *pig-1(gm344)*, *cul-5(ok1706)*, *par-4(it47)*, and *cul-5(ok1706) par-4(it47)* worms were grown 24 h at 20°C before bleaching gravid adults. For the analysis of myosin levels, N2 and *pig-1(gm3444)* L1 were grown at 20°C until adulthood on L4440 or *ani-1(RNAi)* plates (1 mM IPTG) before being bleached. Embryos were then directly resuspended in SDS sample buffer. Western blots were performed according to standard procedures using rabbit anti–PIG-1 (1/5,000; this study), rabbit anti–ANI-2 (residues 890–1015 [Maddox et al., 2005]; 1/2,500), rabbit anti–NMY-2 (residues 945–1368 [Maddox et al., 2005]; 1/5,000; provided by A. Maddox), mouse anti-MLC (T14c, DSHB, 1/2,000), and mouse anti-tubulin (DM1A, 1/2,500; Sigma-Aldrich) antibodies.

Online supplemental material

Fig. S1 shows synthetic lethality between *cul-5*/*rbx-2* and *par-4* mutants, furrow positioning defects upon *par-4* depletion in *cul-5* and *rbx-2* mutants, and ANI-2 levels in *cul-5 par-4* embryonic extracts. Fig. S2 shows quantifications of furrow position in *ani-1(RNAi); par-4* and *ani-2(RNAi); ani-1(RNAi); par-4* embryos and DNA segregation defects in *ani-1(RNAi); par-4* embryos. Fig. S3 shows quantifications of furrow position in *ani-1(RNAi); par-1, pig-1; par-4* and *pig-1; cul-5* embryos as well as ANI-2 localization in *pig-1* embryos. Fig. S4 shows the dynamics of furrow ingression and cortical deformations in *ani-1(RNAi); par-4* embryos. Fig. S5 shows furrow localization in *ani-1(RNAi); par-4* two-cell embryos. Videos 1 and 2 show DIC and confocal recordings of dividing *rbx-2; par-4* and *cul-5 par-4* embryos (depicted in Fig. 1, A and E). Videos 3 and 4 show DIC and confocal recordings of dividing *ani-1(RNAi); par-4* embryos (depicted in Fig. 4, A and D). Video 5 shows the dynamic localization of GFP::PIG-1. Video 6 shows the dynamics of furrow ingression in *ani-1(RNAi); par-4* embryos (depicted in Figs. 6 and S4 A). Video 7 shows the dynamics of cortical myosin accumulation in control and *ani-1(RNAi); par-4* one-cell embryos. Video 8 shows the dynamics of cortical myosin accumulation in control two-cell embryos. Video 9 shows cortical deformations in *ani-1(RNAi); par-4* (depicted in Fig. S4 C) and *nmy-2; ani-1(RNAi); par-4* embryos. Video 10 shows furrow ingression in *rga-3/4(RNAi)* embryos (depicted in Fig. 8 B). Online supplemental material is available at http://www.jcb.org/cgi/content/full/jcb.201503006/DC1. Additional data are available in the JCB DataViewer at http://dx.doi.org/10.1083/jcb.201503006.dv.

Acknowledgments

We would like to thank A. Maddox for providing ANI-2 and NMY-2 antibodies and R. Chan for anti-SPD-1 antibody. Some worm strains were provided by the *Caenorhabidtis* Genetics Center, which is funded by the National Institutes of Health Office of Research Infrastructure Programs (P40 OD010440). N. Loyer helped with furrow tip tracking and E. Daniel and R. Jugele contributed to the earlier steps of this project. We thank M. Gotta, in whose laboratory this project was initiated, and the Microscopy Rennes Imaging Center for assistance with microscopy. We would also like to thank R. Le Borgne, S. Le Bras, L. Chesneau, S. Dixon, A. Echard, G. Gillard, and J. Pécreaux for discussions and critical reading of the manuscript.

A. Pacquelet was supported by the Institut National de la Santé et de la Recherche Médicale and a Stratégie d'attractivité durable grant from the Région Bretagne and our group is supported by the Ligue contre le cancer (22/29/35/72), the Centre National de la Recherche Scientifique, and the Université Rennes 1.

The authors declare no competing financial interests.

Submitted: 2 March 2015
Accepted: 19 August 2015

References

Amini, R., E. Goupil, S. Labella, M. Zetka, A.S. Maddox, J.C. Labbé, and N.T. Chartier. 2014. *C. elegans* Anillin proteins regulate intercellular bridge stability and germline syncytial organization. *J. Cell Biol.* 206:129–143. http://dx.doi.org/10.1083/jcb.201310117

Basant, A., S. Lekomtsev, Y.C. Tse, D. Zhang, K.M. Longhini, M. Petronczki, and M. Glotzer. 2015. Aurora B kinase promotes cytokinesis by inducing centralspindlin oligomers that associate with the plasma membrane. *Dev. Cell.* 33:204–215. http://dx.doi.org/10.1016/j.devcel.2015.03.015

Benkemoun, L., C. Descoteaux, N.T. Chartier, L. Pintard, and J.C. Labbé. 2014. PAR-4/LKB1 regulates DNA replication during asynchronous division of the early *C. elegans* embryo. *J. Cell Biol.* 205:447–455. http://dx.doi.org/10.1083/jcb.201312029

Bringmann, H., C.R. Cowan, J. Kong, and A.A. Hyman. 2007. LET-99, GOA-1/GPA-16, and GPR-1/2 are required for aster-positioned cytokinesis. *Curr. Biol.* 17:185–191. http://dx.doi.org/10.1016/j.cub.2006.11.070

Cabernard, C., K.E. Prehoda, and C.Q. Doe. 2010. A spindle-independent cleavage furrow positioning pathway. *Nature.* 467:91–94. http://dx.doi.org/10.1038/nature09334

Chartier, N.T., D.P. Salazar Ospina, L. Benkemoun, M. Mayer, S.W. Grill, A.S. Maddox, and J.C. Labbé. 2011. PAR-4/LKB1 mobilizes nonmuscle myosin through anillin to regulate *C. elegans* embryonic polarization and cytokinesis. *Curr. Biol.* 21:259–269. http://dx.doi.org/10.1016/j.cub.2011.01.010

Chartrain, I., A. Couturier, and J.P. Tassan. 2006. Cell-cycle-dependent cortical localization of pEg3 protein kinase in *Xenopus* and human cells. *Biol. Cell.* 98:253–263. http://dx.doi.org/10.1042/BC20050041

Chien, S.C., E.M. Brinkmann, J. Teuliere, and G. Garriga. 2013. *Caenorhabditis elegans* PIG-1/MELK acts in a conserved PAR-4/LKB1 polarity pathway to promote asymmetric neuroblast divisions. *Genetics.* 193:897–909. http://dx.doi.org/10.1534/genetics.112.148106

Cordes, S., C.A. Frank, and G. Garriga. 2006. The *C. elegans* MELK ortholog PIG-1 regulates cell size asymmetry and daughter cell fate in asymmetric neuroblast divisions. *Development.* 133:2747–2756. http://dx.doi.org/10.1242/dev.02447

D'Agostino, I., C. Merritt, P.L. Chen, G. Seydoux, and K. Subramaniam. 2006. Translational repression restricts expression of the *C. elegans* Nanos homolog NOS-2 to the embryonic germline. *Dev. Biol.* 292:244–252. http://dx.doi.org/10.1016/j.ydbio.2005.11.046

Dechant, R., and M. Glotzer. 2003. Centrosome separation and central spindle assembly act in redundant pathways that regulate microtubule density and trigger cleavage furrow formation. *Dev. Cell.* 4:333–344. http://dx.doi.org/10.1016/S1534-5807(03)00057-1

Grill, S.W., P. Gönczy, E.H. Stelzer, and A.A. Hyman. 2001. Polarity controls forces governing asymmetric spindle positioning in the *Caenorhabditis elegans* embryo. *Nature.* 409:630–633. http://dx.doi.org/10.1038/35054572

Kamath, R.S., A.G. Fraser, Y. Dong, G. Poulin, R. Durbin, M. Gotta, A. Kanapin, N. Le Bot, S. Moreno, M. Sohrmann, et al. 2003. Systematic functional analysis of the *Caenorhabditis elegans* genome using RNAi. *Nature.* 421:231–237. http://dx.doi.org/10.1038/nature01278

Kamura, T., K. Maenaka, S. Kotoshiba, M. Matsumoto, D. Kohda, R.C. Conaway, J.W. Conaway, and K.I. Nakayama. 2004. VHL-box and SOCS-box domains determine binding specificity for Cul2-Rbx1 and Cul5-Rbx2 modules of ubiquitin ligases. *Genes Dev.* 18:3055–3065. http://dx.doi.org/10.1101/gad.1252404

Kemphues, K. 2000. PARsing embryonic polarity. *Cell.* 101:345–348. http://dx.doi.org/10.1016/S0092-8674(00)80844-2

Kemphues, K.J., J.R. Priess, D.G. Morton, and N.S. Cheng. 1988. Identification of genes required for cytoplasmic localization in early *C. elegans* embryos. *Cell.* 52:311–320. http://dx.doi.org/10.1016/S0092-8674(88)80024-2

Knoblich, J.A. 2010. Asymmetric cell division: recent developments and their implications for tumour biology. *Nat. Rev. Mol. Cell Biol.* 11:849–860. http://dx.doi.org/10.1038/nrm3010

Le Page, Y., I. Chartrain, C. Badouel, and J.P. Tassan. 2011. A functional analysis of MELK in cell division reveals a transition in the mode of cytokinesis during *Xenopus* development. *J. Cell Sci.* 124:958–968. http://dx.doi.org/10.1242/jcs.069567

Lewellyn, L., J. Dumont, A. Desai, and K. Oegema. 2010. Analyzing the effects of delaying aster separation on furrow formation during cytokinesis in the *Caenorhabditis elegans* embryo. *Mol. Biol. Cell.* 21:50–62. http://dx.doi.org/10.1091/mbc.E09-01-0089

Lizcano, J.M., O. Göransson, R. Toth, M. Deak, N.A. Morrice, J. Boudeau, S.A. Hawley, L. Udd, T.P. Mäkelä, D.G. Hardie, and D.R. Alessi. 2004. LKB1 is a master kinase that activates 13 kinases of the AMPK subfamily, including MARK/PAR-1. *EMBO J.* 23:833–843. http://dx.doi.org/10.1038/sj.emboj.7600110

Maddox, A.S., B. Habermann, A. Desai, and K. Oegema. 2005. Distinct roles for two *C. elegans* anillins in the gonad and early embryo. *Development.* 132:2837–2848. http://dx.doi.org/10.1242/dev.01828

Morton, D.G., J.M. Roos, and K.J. Kemphues. 1992. par-4, a gene required for cytoplasmic localization and determination of specific cell types in *Caenorhabditis elegans* embryogenesis. *Genetics.* 130:771–790.

Morton, D.G., W.A. Hoose, and K.J. Kemphues. 2012. A genome-wide RNAi screen for enhancers of par mutants reveals new contributors to early embryonic polarity in *Caenorhabditis elegans*. *Genetics.* 192:929–942. http://dx.doi.org/10.1534/genetics.112.143727

Motegi, F., S. Zonies, Y. Hao, A.A. Cuenca, E. Griffin, and G. Seydoux. 2011. Microtubules induce self-organization of polarized PAR domains in *Caenorhabditis elegans* zygotes. *Nat. Cell Biol.* 13:1361–1367. http://dx.doi.org/10.1038/ncb2354

Munro, E., J. Nance, and J.R. Priess. 2004. Cortical flows powered by asymmetrical contraction transport PAR proteins to establish and maintain anterior-posterior polarity in the early *C. elegans* embryo. *Dev. Cell.* 7:413–424. http://dx.doi.org/10.1016/j.devcel.2004.08.001

Nishimura, Y., and S. Yonemura. 2006. Centralspindlin regulates ECT2 and RhoA accumulation at the equatorial cortex during cytokinesis. *J. Cell Sci.* 119:104–114. http://dx.doi.org/10.1242/jcs.02737

Ou, G., N. Stuurman, M. D'Ambrosio, and R.D. Vale. 2010. Polarized myosin produces unequal-size daughters during asymmetric cell division. *Science.* 330:677–680. http://dx.doi.org/10.1126/science.1196112

Piekny, A.J., and M. Glotzer. 2008. Anillin is a scaffold protein that links RhoA, actin, and myosin during cytokinesis. *Curr. Biol.* 18:30–36. http://dx.doi.org/10.1016/j.cub.2007.11.068

Piekny, A.J., and A.S. Maddox. 2010. The myriad roles of Anillin during cytokinesis. *Semin. Cell Dev. Biol.* 21:881–891. http://dx.doi.org/10.1016/j.semcdb.2010.08.002

Raich, W.B., A.N. Moran, J.H. Rothman, and J. Hardin. 1998. Cytokinesis and midzone microtubule organization in *Caenorhabditis elegans* require the kinesin-like protein ZEN-4. *Mol. Biol. Cell.* 9:2037–2049. http://dx.doi.org/10.1091/mbc.9.8.2037

Roth, M., C. Roubinet, N. Iffländer, A. Ferrand, and C. Cabernard. 2015. Asymmetrically dividing *Drosophila* neuroblasts utilize two spatially and temporally independent cytokinesis pathways. *Nat. Commun.* 6:6551. http://dx.doi.org/10.1038/ncomms7551

Sasagawa, Y., S. Sato, T. Ogura, and A. Higashitani. 2007. *C. elegans* RBX-2-CUL-5- and RBX-1-CUL-2-based complexes are redundant for oogenesis and activation of the MAP kinase MPK-1. *FEBS Lett.* 581:145–150. http://dx.doi.org/10.1016/j.febslet.2006.12.009

Schmutz, C., J. Stevens, and A. Spang. 2007. Functions of the novel RhoGAP proteins RGA-3 and RGA-4 in the germ line and in the early embryo

of *C. elegans*. *Development.* 134:3495–3505. http://dx.doi.org/10.1242/dev.000802

Severson, A.F., D.R. Hamill, J.C. Carter, J. Schumacher, and B. Bowerman. 2000. The aurora-related kinase AIR-2 recruits ZEN-4/CeMKLP1 to the mitotic spindle at metaphase and is required for cytokinesis. *Curr. Biol.* 10:1162–1171. http://dx.doi.org/10.1016/S0960-9822(00)00715-6

Tenlen, J.R., J.N. Molk, N. London, B.D. Page, and J.R. Priess. 2008. MEX-5 asymmetry in one-cell *C. elegans* embryos requires PAR-4- and PAR-1-dependent phosphorylation. *Development.* 135:3665–3675. http://dx.doi.org/10.1242/dev.027060

Tse, Y.C., M. Werner, K.M. Longhini, J.C. Labbe, B. Goldstein, and M. Glotzer. 2012. RhoA activation during polarization and cytokinesis of the early *Caenorhabditis elegans* embryo is differentially dependent on NOP-1 and CYK-4. *Mol. Biol. Cell.* 23:4020–4031. http://dx.doi.org/10.1091/mbc.E12-04-0268

Verbrugghe, K.J., and J.G. White. 2004. SPD-1 is required for the formation of the spindle midzone but is not essential for the completion of cytokinesis in *C. elegans* embryos. *Curr. Biol.* 14:1755–1760. http://dx.doi.org/10.1016/j.cub.2004.09.055

Watts, J.L., D.G. Morton, J. Bestman, and K.J. Kemphues. 2000. The *C. elegans* par-4 gene encodes a putative serine-threonine kinase required for establishing embryonic asymmetry. *Development.* 127:1467–1475.

Werner, M., E. Munro, and M. Glotzer. 2007. Astral signals spatially bias cortical myosin recruitment to break symmetry and promote cytokinesis. *Curr. Biol.* 17:1286–1297. http://dx.doi.org/10.1016/j.cub.2007.06.070

Yüce, O., A. Piekny, and M. Glotzer. 2005. An ECT2–centralspindlin complex regulates the localization and function of RhoA. *J. Cell Biol.* 170:571–582. http://dx.doi.org/10.1083/jcb.200501097